Investigation of how Reflected Radiation due to Non-Uniform Grids Perturbs Solutions Computed with Finite Difference Methods

S. Walter
Supervisor: Tomas Dohnal
ETH Zürich

August, 2006

Abstract

We investigate the behavior of solutions to the 1D NonLinear Coupled Mode Equations (NLCME) with a Finite Difference (FD) method. The FD approach is used to render the NLCMEs a system of Ordinary Differential Equations (ODE) that is then solved with a splitting method. The high frequency components of the solution moving from a fine grid into a coarse grid cannot be resolved on the coarse grid and are reflected back into the fine region. Collision of two gap solitons produces high frequency radiation that travels faster than the gap solitons. This report investigates to what extend this reflected radiation perturbs the solution in the fine gird region and how fine the grid in the coarse region should be to neglect the resulting error. We observe that the properties of the reflected radiation depend on the FD approximation. We also test the conservation energy and Hamiltonian and compare it to Runge-Kutta methods, as well as the order in the timestep dt and the grid spacing h of the used method. We observe superconvergence, i.e., in the L^2-norm the order was 4 when we expect it to be of second order. Additionally, with our used method we could not reproduce the results from Ref. [1], as for example the merger of two gap solitons. This is probably due to the dissipative nature of the upwinding FD approximation.

KEYWORDS: FD, HAMILTONIAN, NON-UNIFORM GRID, NLCME, GAP SOLITONS, COLLISION

1 Introduction

One method to treat partial differential equations (PDE) is the *finite difference method*, i.e. all derivatives are discretized with a finite difference formula (FD). Given the starting conditions, the evolution of the solution can be solved numerically. The computations are performed on a grid in a finite region. The finer the grid and the larger the region the longer the runtime of the simulation. To save computation time one can use a non-equidistant grid; fine in the region of interest and coarse in the other regions. If the solution propagates into the coarse region, the high frequencies are reflected back into the fine grid region since they cannot be resolved on the coarse grid (similarly to the Nyquist-Shannon sampling theorem [6]). These reflections perturb the solution in the region of interest.

The goal of this term project is to investigate the NLCME (Eqn. (1)) with gap solitons (Eqn. (3)) as starting conditions. The NLCME describe the physical setup of a Bragg grating. Bragg gratings are waveguides with a periodic variation of the refractive index. The dynamics evolve from an interplay between the Bragg grating induced effective dispersion and the Kerr non-linearity of the waveguide material. We let two gap solitons collide whereupon radiation is produced that travels faster than the solitons. Since only the colliding gap solitons are of interest, the fine mesh covers only the region where the gap solitons exist. At the transition between fine and coarse grid this radiation is reflected back and perturbs the solution in the fine region. We are interested in how fine the grid in the coarse region must be such that the error is negligible.

In Section 2 we introduce the nonlinear coupled mode equations (NLCME) and one class of solutions: the gap solitons. Section 3 explains the numerical techniques we have used to solve the NLCME,

while Section 4 focuses on their implementation. In Section 5 one can find the results and discussion of the performed simulations, namely the analysis of error convergence in the time step dt (Section 5.4) and the spatial grid width h (Section 5.3), in Section 5.1 a comparison between the 2^{nd} resp. 4^{th} order Runge-Kutta method and the splitting method (centered FD). In Subsection 5.6 we present the results we have obtained by colliding two solitons in a region with a fine grid and a coarse grid of varying h in the outer regions.

2 The Model

We investigate the Nonlinear Coupled Mode Equations (NLCME)

$$
\begin{aligned}
i(\dot{E} + v_G E') + \kappa F + \Gamma(|E|^2 + 2|F|^2)E &= 0 \qquad (1)\\
i(\dot{F} - v_G F') + \kappa E + \Gamma(|F|^2 + 2|E|^2)F &= 0\,, \qquad (2)
\end{aligned}
$$

where $E' \equiv \partial_x E$ is the spatial partial derivative and $\dot{E} \equiv \partial_t E$ the partial time derivative. The parameters κ, $\Gamma \in \mathbb{R}$ and $v_G > 0$ represent the physical setup and are fixed. The NLCME have a class of solutions, the so-called *gap solitons* which are in fact solitary waves, but not true solitons, i.e., collision of two gap solitons changes their shape. They are defined by the right traveling wave E and the left traveling wave F:

$$
\begin{aligned}
E &= s\alpha e^{i\eta}\sqrt{|\frac{\kappa}{2\Gamma}|}\frac{1}{\Delta}\sin(\delta)e^{is\sigma}\operatorname{sech}(\theta - is\delta/2) \qquad (3)\\
F &= -\alpha e^{i\eta}\sqrt{|\frac{\kappa}{2\Gamma}|}\Delta\sin(\delta)e^{is\sigma}\operatorname{sech}(\theta + is\delta/2)\,, \qquad (4)
\end{aligned}
$$

where

$$
\begin{aligned}
\gamma &= \frac{1}{\sqrt{1-v^2}} & \qquad \Delta &= \left(\frac{1-v}{1+v}\right)^{\frac{1}{4}}\\
\theta &= \gamma\kappa sin(\delta)(v_G^{-1}x - vt) & \qquad \sigma &= \gamma\kappa cos(\delta)(v_G^{-1}vx - t)\\
s &= \operatorname{sign}(\kappa\Gamma) & \qquad \alpha &= \sqrt{\frac{2(1-v^2)}{3-v^2}}\,.\\
e^{i\eta} &= \left(-\frac{e^{2\theta} + e^{-is\delta}}{e^{2\theta} + e^{is\delta}}\right)^{\frac{2v}{3-v^2}}
\end{aligned}
$$

The parameter $v \in (0, v_G)$ defines the velocity at which the soliton propagates and $\delta \in [0, \pi]$ defines the soliton width and amplitude. It is proportional to the energy $\mathcal{E} = \int_{-\infty}^{\infty} |E(x)|^2 + |F(x)|^2 dx = 8\delta\sqrt{1+v^2}(3+v^2)^{-1}$. We rewrite the NLCME as

$$
\begin{aligned}
\begin{pmatrix} \dot{E} \\ \dot{F} \end{pmatrix} &= \underbrace{\begin{pmatrix} -v_G E' + i\kappa F \\ v_G F' + i\kappa E \end{pmatrix}}_{\mathrm{L}(E,F)} + \underbrace{\begin{pmatrix} i\Gamma(|E|^2 + 2|F|^2)E \\ i\Gamma(|F|^2 + 2|E|^2)F \end{pmatrix}}_{\mathrm{NL}(E,F)}\,, \qquad (5)\\
\Leftrightarrow \qquad \dot{y} &= f(y, y')\,. \qquad (6)
\end{aligned}
$$

2.1 The Hamiltonian

The NLCME are Hamiltonian, i.e. they are equivalent to

$$
\begin{aligned}
\dot{E} &= i\frac{\delta H}{\delta E^*} \qquad (7)\\
\dot{F} &= i\frac{\delta H}{\delta F^*}\,. \qquad (8)
\end{aligned}
$$

If the Hamiltonian H is real, the equations are also equivalent to $\dot{E}^* = -i\frac{\delta H}{\delta E}$ (F respectively). $\frac{\delta f[g]}{\delta g}$ denotes the functional derivative of the functional f of the function g. The corresponding (real) Hamiltonian to the NLCME is

$$H = \int_{\mathbb{R}} i(E^*E' - F^*F') + \kappa(FE^* + F^*E) + \Gamma(\frac{1}{2}|E|^4 + 2|E|^2|F|^2 + \frac{1}{2}|F|^4)dx \; . \tag{9}$$

Hamiltonian systems have the property that the Hamiltonian is conserved quantity. For our system, additionally the energy $\mathcal{E} = \int_{\mathbb{R}} |E(x)|^2 + |F(x)|^2 dx$ is a conserved quantity in time. If the system is Hamiltonian, then the flow is symplectic (Theorem 2.6 from Reference [5]). If ϕ_t is the flow of the system, then the flow is called *symplectic* if $\left(\frac{\partial \phi_t}{\partial y^0}\right)^T J \left(\frac{\partial \phi_t}{\partial y^0}\right) = J$, where $J = (0, \mathrm{Id}; -\mathrm{Id}, 0)$. A numerical method is called *symplectic* if the one-step map $y^1 = \Phi_{dt}(y^0)$ is symplectic when applied to a Hamiltonian system. We use the notation Φ for numerical methods and ϕ for the exact analytical solution and y^k for the solution at timestep k.

3 The Used Numerical Techniques to Solve the NLCME

3.1 The Splitting Method

We follow the argumentation of Chapter II.5 "Splitting Methods" of Ref. [5]. The idea of the *splitting method* is to separate the vector field of an ODE into integrable parts, i.e.

$$\dot{y} = f(y) = f^{[1]}(y) + f^{[2]}(y) \; . \tag{10}$$

The flow of the system is then approximated by propagating with the flow of the vector field $f^{[1]}(y)$ for a short period of time dt and then propagate with the flow of the vector field $f^{[2]}(y)$. The methods can be seen in Figure 1 (a) and are of first order. Using theorem 4.1 from Chapter II.4 "Composition Methods" a symmetric method of second order can be constructed. This results in

$$\Phi_{dt} = \phi^{[1]}_{dt/2} \circ \phi^{[2]}_{dt} \circ \phi^{[1]}_{dt/2} \; . \tag{11}$$

An illustration of this splitting idea can be found in Fig. 1. We remark that the splitting has the property that if $\Phi^{[1]}$ and $\Phi^{[2]}$ symplectic flows, then Φ is also symplectic.

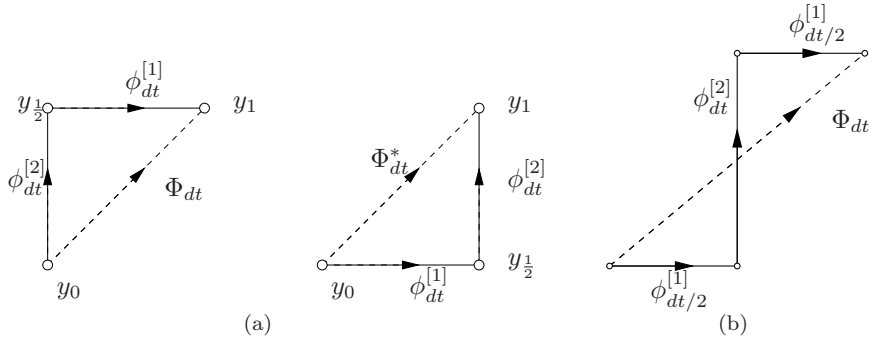

Figure 1: Splitting methods. In a) and b) splittings of order $\mathcal{O}(dt)$ are depicted. The combined symmetric method in c) is of order $\mathcal{O}(dt^2)$.

3.2 Derivation of a Second Order Centered Finite Difference Formula for the First Derivative on Non-Equidistant Grids

We define $h_k = x_k - x_{k-1}$ and $\frac{du}{dx}(x_k) = u'_k$, $y_k = y(x_k)$. We make a Taylor expansion of y_{k+1} and y_{k-1} around x_k:

$$\begin{aligned} y_{k+1} - y_k &= y'_k h_{k+1} + \frac{1}{2} y''_k h_{k+1}^2 + \frac{1}{6} y'''_k h_{k+1}^3 + \mathcal{O}(h_{k+1}^4) \\ y_{k-1} - y_k &= -y'_k h_k + \frac{1}{2} y''_k h_k^2 - \frac{1}{6} y'''_k h_k^3 + \mathcal{O}(h_k^4) \ . \end{aligned}$$

We use a linear combination of the above equations to eliminate the second derivative terms. Multiplication of the first equation with $\frac{1}{h_{k+1}^2}$ and $\frac{1}{h_k^2}$ with the second equation and subtraction of the equation results in

$$\begin{aligned} y'_k + \frac{1}{6} y'''_k h_k h_{k+1} + \mathcal{O}(h^3) &= \frac{h_k}{h_{k+1}(h_k + h_{k+1})}(y_{k+1} - y_k) - \frac{h_{k+1}}{h_k(h_k + h_{k+1})}(y_{k-1} - y_k) \\ y'_k + \mathcal{O}(h^2) &= A_k(y_{k+1} - y_k) + B_k(y_k - y_{k-1}) \ , \end{aligned} \tag{12}$$

where $A_k = \frac{h_k}{h_{k+1}(h_k+h_{k+1})}$, $B_k = \frac{h_{k+1}}{h_k(h_k+h_{k+1})}$ and $h = max(h_k, h_{k+1})$.

3.3 Derivation of a Second Order Upwinding Finite Difference Formula for the First Derivative on Non-Equidistant Grids

To derive the forward upwinding formula, we start with

$$\begin{aligned} y_{k+1} &= y_k + y'_k h_{k+1} + \frac{1}{2} y''_k h_{k+1}^2 + \mathcal{O}(h_{k+1}^3) \\ y_{k+2} &= y_k + y'_k (h_{k+1} + h_{k+2}) + \frac{1}{2} y''_k (h_{k+1} + h_{k+2})^2 + \mathcal{O}((h_{k+1} + h_{k+2})^3) \ . \end{aligned}$$

Multiplication of the upper/lower Equation with $(h_{k+1}+h_{k+2})$ and h_{k+1} respectively and a subtraction results in

$$y'_k = -(B_k + A_k) y_k + A_k y_{k+1} + B_k y_{k+2} + \mathcal{O}(h^2) \ , \tag{13}$$

where $A_k \equiv \frac{h_{k+1}+h_{k+2}}{h_{k+1}h_{k+2}}$,$B_k \equiv -\frac{h_{i+1}}{(h_{k+1}+h_{k+2})h_{i+2}}$, $h_{k+1} = x_{k+1} - x_k$ and $h = \max(h_{k+1}, h_{k+2})$
The derivation of the backward upwinding formula results in

$$y'_k = -C_k y_{k-1} - D_k y_{k-2} + (C_k + D_k) y_k + \mathcal{O}(h^2) \ , \tag{14}$$

where $C_k \equiv \frac{h_{k-1}+h_{k-2}}{h_{k-1}h_{k-2}}$, $D_k \equiv -\frac{h_{k-1}}{(h_{k-1}+h_{k-2})h_{k-2}}$ and $h = \max(h_{k-1}, h_{k-2})$.

4 Implementation

The goal is to find a good numerical method to solve the NLCME equations, if possible a symplectic method as the governing PDE system is Hamiltonian. To solve Eqn. (5) we use the splitting method from Section 3.1, i.e.,

$$\begin{aligned} \dot{y} &= f(y) = f^{[1]}(y) + f^{[2]}(y) \\ f^{[1]}(y) &= \mathrm{NL}(y) \\ f^{[2]}(y) &= \mathrm{L}(y) \ . \end{aligned}$$

The flow of the vector field $L(E, F)$ resp. $\mathrm{NL}(E, F)$ is denoted ϕ^{L} resp. ϕ^{NL}. Then the numerical flow of Eqn. (5) is

$$\Phi_{dt} = \phi^{\mathrm{NL}}_{dt/2} \circ \phi^{\mathrm{L}}_{dt} \circ \phi^{\mathrm{NL}}_{dt/2} \ . \tag{15}$$

4.1 Performing a Split-Step along the Vector Field of the Non-Linear Part

We can solve the non-linear part $\dot{y} = \mathrm{NL}(y)$ analytically. The numerical flow is given by

$$\phi^{\mathrm{NL}}_t(E(x,0), F(x,0)) = \begin{pmatrix} e^{i\Gamma(|E(x,0)|^2 + 2|F(x,0)|^2)t} E(x,0) \\ e^{i\Gamma(|F(x,0)|^2 + 2|E(x,0)|^2)t} F(x,0) \end{pmatrix} \ . \tag{16}$$

4.2 Split-Step along the Vector Field of the Linear Part

We cannot solve the linear part analytically. We use a FD formula to discretize the spatial derivative ∂_x. For few time steps a second order centered finite difference formula and for long runtimes with many time steps a second order upwinding finite difference formula. The reason for that is that the centered FD approximation results in better energy and Hamiltonian conservation than the upwinding FD approximation. However, as discussed in Section 5.2, the centered FD approximation is instable because of decoupling between solutions on even/odd grid points. We therefore use the upwinding FD approximation for long runtimes.

4.2.1 Split-Step with the Centered Finite Difference Formula

We discretize $\partial_x u$ with

$$y_k' = A_k(y_{k+1} - y_k) + B_k(y_k - y_{k-1}) + \mathcal{O}(h^2) \,, \tag{17}$$

where $A_k = \frac{h_k}{h_{k+1}(h_k+h_{k+1})}$, $B_k = \frac{h_{k+1}}{h_k(h_k+h_{k+1})}$, $h_k = x_k - x_{k-1}$, $y_k = E(x_k,t)$ or $y_k = F(x_k,t)$ on the non-equidistant grid $(x_1,\ldots,x_N)$. Therefore, the linear part of the system of ODEs we have to solve is

$$\dot{y}_k \equiv \begin{pmatrix} \dot{E}_k \\ \dot{F}_k \end{pmatrix} = \underbrace{\begin{pmatrix} -v_G A_k E_{k+1} - v_G(-A_k+B_k)E_k + v_G B_k E_{k-1} + i\kappa F_k \\ v_G A_k F_{k+1} + v_G(-A_k+B_k)F_k - v_G B_k F_{k-1} + i\kappa E_k \end{pmatrix}}_{\equiv \mathrm{L}(E,F)} . \tag{18}$$

The index k is $\in [1,N]$. As boundary condition we use $(E_1,F_1) = (E_N,F_N) = (0,0)$. We define

$$(z_1,z_2,z_3,z_4,\ldots,z_{2N-1},z_{2N}) = (E_1,F_1,E_2,F_2,\ldots,E_N,F_N) \,. \tag{19}$$

Since $\mathrm{L}(E,F)$ is linear, we can write it as matrix

$$\dot{z} = M_\mathrm{L} z \,, \tag{20}$$

where $M_\mathrm{L} \in \mathbb{C}^{2N\times 2N}$. Because of the boundary conditions it follows that $(\dot{E}_1,\dot{F}_1) = (\dot{E}_N,\dot{F}_N) = (0,0)$, i.e., the first two and the last two rows are all zero. To find the matrix elements we need to consider two cases:

l is even Then z_l is always F_k with $k = \frac{l}{2}$.

$$\dot{z}_l = -v_G B_k z_{l-2} + i\kappa z_{l-1} + v_G(-A_k+B_k)z_l + v_G A_k z_{l+2} \tag{21}$$

l is odd : Then z_l is always E_k with $k = \frac{l+1}{2}$.

$$\dot{z}_l = v_G B_k z_{l-2} - v_G(-A_k+B_k)z_l + i\kappa z_{l+1} - v_G A_k z_{l+2} \tag{22}$$

With these equation we can compute the matrix elements of the matrix $M_\mathrm{L}(3:2N-2,1:2N)$. Since the first and last two elements in z are zero, the first and last two columns do not contribute. Therefore, the whole dynamics of the system are represented by $w = z(3:2N-2)$ and $\tilde{M}_\mathrm{L} = M_\mathrm{L}(3:2N-2,3:2N-2)$, i.e.,

$$\dot{w} = \tilde{M}_\mathrm{L} w \,. \tag{23}$$

4.2.2 Split-Step with the Upwinding Finite Difference Formula

Since E is potentially the right moving solution and F the left moving solution we use the backward finite difference formula for E and the forward finite difference formula for F. That means

$$\dot{y}_k \equiv \begin{pmatrix} \dot{E}_k \\ \dot{F}_k \end{pmatrix} = \underbrace{\begin{pmatrix} -v_G(-C_k E_{k-1} - D_k E_{k-2} + (C_k+D_k)E_k) + i\kappa F_k \\ v_G(-(B_k+A_k)F_k + A_k F_{k+1} + B_k F_{k+2}) + i\kappa E_k \end{pmatrix}}_{\equiv \mathrm{L}(E,F)} , \tag{24}$$

where $A_k \equiv \frac{h_{k+1}+h_{k+2}}{h_{k+1}h_{k+2}}$,$B_k \equiv -\frac{h_{i+1}}{(h_{k+1}+h_{k+2})h_{i+2}}$, $C_k \equiv \frac{h_{k-1}+h_{k-2}}{h_{k-1}h_{k-2}}$, $D_k \equiv -\frac{h_{k-1}}{(h_{k-1}+h_{k-2})h_{k-2}}$ and $h_{k+1} = x_{k+1} - x_k$. To build the matrix we consider again the two cases

l **is even** Then z_l is always F_k with $k = \frac{l}{2}$.

$$\dot{z}_l = i\kappa z_{l-1} - v_G(A_k + B_k)z_l + v_G A_k z_{l+2} + v_G B_k z_{l+4} \tag{25}$$

l **is odd** : Then z_l is always E_k with $k = \frac{l+1}{2}$.

$$\dot{z}_l = v_G D_k z_{l-4} + v_G C_k z_{l-2} - v_G(C_k + D_k)z_l + i\kappa z_{l+1} \tag{26}$$

4.2.3 The Implicit Midpoint Rule for the Time Integration

Once $\tilde{M}_{\mathrm{L}}$ is built, we have a big system of coupled ODEs that we have to solve. Since the NLCMEs are Hamiltonian, we hope that their discretized version is still,at least approximately, Hamiltonian. We hope to find an approximately symplectic method and therefore use the (symplectic) implicit midpoint rule to integrate these equations of motion, i.e.,

$$w^{n+1} = w^n + dt\tilde{M}_{\mathrm{L}}(\frac{w^{n+1}+w^n}{2}) \tag{27}$$

$$\Leftrightarrow \quad (\mathrm{Id} - \frac{1}{2}dt\ \tilde{M}_{\mathrm{L}})w^{n+1} = (\mathrm{Id} + \frac{1}{2}dt\ \tilde{M}_{\mathrm{L}})w^n\ . \tag{28}$$

4.3 Computing the Hamiltonian and the Energy $\mathcal{E}$

In the simulations the value of the Hamiltonian has to be computed. To do so, we discretize the spatial derivative with the centered FD formula. We write

$$H = \int_{\mathbb{R}} \mathrm{int}(E, F, E', F')dx\ , \tag{29}$$

where

$$\begin{aligned}
\mathrm{int}(E, F, E', F') &= i(E^*E' - F^*F') + \kappa(FE^* + F^*E) + \Gamma(\frac{1}{2}|E|^4 + 2|E|^2|F|^2 + \frac{1}{2}|F|^4) \\
\mathrm{int}(E(x_k), F(x_k), E'(x_k), F'(x_k)) &\approx i\{E_k^*[A_k(E_{k+1} - E_k) + B_k(E_k - E_{k-1})] \\
&\quad -F_k^*[A_k(F_{k+1} - F_k) + B_k(F_k - F_{k-1})]\} \\
&\quad +\kappa(F_kE_k^* + F_k^*E_k) + \Gamma(\frac{1}{2}|E_k|^4 + 2|E_k|^2|F_k|^2 + \frac{1}{2}|F_k|^4)dx\ .
\end{aligned} \tag{30}$$

For the integration we have used the trapezoidal rule, i.e.,

$$H = \frac{1}{2}\sum_k (x_k - x_{k-1})(\mathrm{int}_k + \mathrm{int}_{k-1})\ . \tag{31}$$

The energy $\mathcal{E}$ is analogously computed by $\mathcal{E}_k = |E_k|^2 + |F_k|^2$ and

$$\mathcal{E} = \frac{1}{2}\sum_k (x_k - x_{k-1})(\mathcal{E}_k + \mathcal{E}_{k-1})\ . \tag{32}$$

5 Results and Discussion

Throughout this discussion we have used the parameters $v_G = 1$, $\Gamma = 0.5$ and $\kappa = 1$. At first we perform tests on the two splitting method variants, namely the computation of the order in dt and h. Also, a comparison between the splitting method (centered FD) and a 2^{nd} resp. 4^{th} order Runge-Kutta method is made. The reason why two different FD formulas are considered is the instability of the centered FD splitting method; although it conserves the energy $\mathcal{E}$ and Hamiltonian H much better than the upwinding FD splitting method. For the simulation of collisions between two solitons long runtimes with many time steps are necessary. We therefore use the upwinding FD splitting method for the purpose to investigate the influence of reflected radiation in the region of interest.

5.1 Comparison between the Runge-Kutta Method and Splitting Method

At first we compare the second order splitting method (centered FD) with a fourth order Runge-Kutta method. The measurements have been taken with the following parameters T_start = 0 , T_end =20, time steps =400, N=1000, x_left=-5, x_right=25. The computation time for the Runge-Kutta method is 82.23 seconds while the split step methods finishes in 4.67 seconds. The evolution of the energy and the Hamiltonian can be seen in Figure 2. The Butcher table of the fourth order method can be found in Table 1.

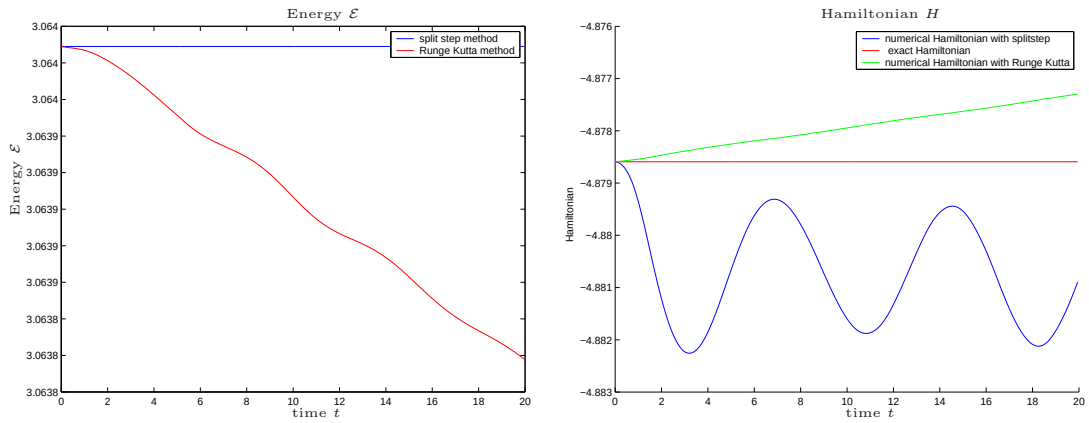

(a) (b)

Figure 2: Comparison of the 4$^{\text{th}}$ order Runge-Kutta with the splitting method (centered FD).

In another measurement we compare a second order Runge-Kutta method with the splitting method (centered FD). The simulation has been performed with the parameters T_start = 0, T_end =15, time steps =2000, N=1000, x_left=-5, x_right=25. The result can be seen in Figure 3. The runtime for the splitting method (centered FD) was 20.59 seconds resp. 194.79 seconds for the second order Runge-Kutta method. The corresponding Butcher table can also be found in Table 1.

The splitting method (centered FD) yields good results even with much short computation time compared to the Runge-Kutta methods.

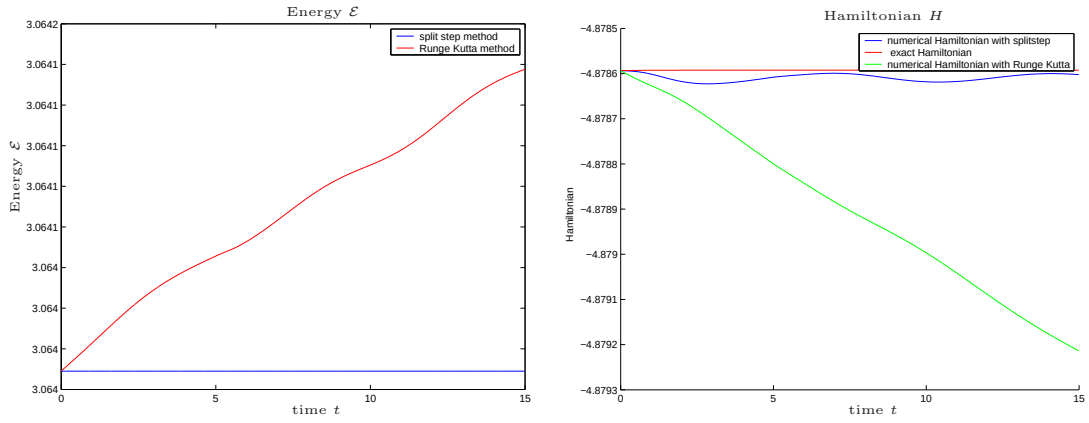

(a) (b)

Figure 3: Comparison of the 2$^{\text{nd}}$ order Runge-Kutta with the splitting method (centered FD). One can see that the splitting method (centered FD) seems approximately symplectic while the the Hamiltonian diverges with the Runge-Kutta method. Also, the Runge-Kutta method does not conserve the energy.

0		
1	1	
	1/2	1/2

0				
1/2	1/2			
1/2	0	1/2		
1	0	0	1	
	1/6	2/6	2/6	1/6

Table 1: On the left the Butcher table of the 2^{nd} order Runge-Kutta method and on the right of the 4^{th} order.

5.2 Comparison Between the Upwinding FD Splitting Method and the Centered FD Splitting Method

In Figure 4 one can see that the centered FD splitting method is instable. After some time steps high frequency oscillations occur that are not physical. These oscillations appear because of even/odd grid points decoupling. In Figure 5 we compare the centered FD splitting method with the upwinding FD splitting method which is stable. The centered FD version has better properties concerning the conservation of energy and Hamiltonian [a), b) resp. c),d)] but already shows for the used runtime the beginning instability (Figure 5 a)). In e) and f) the time evolution of the numerical solution is plotted together with the exact solution. The centered FD approximation lags behind, but conserves roughly the shape and amplitude of the pulse, whereas the upwinding FD version doesn't conserve shape or amplitude.

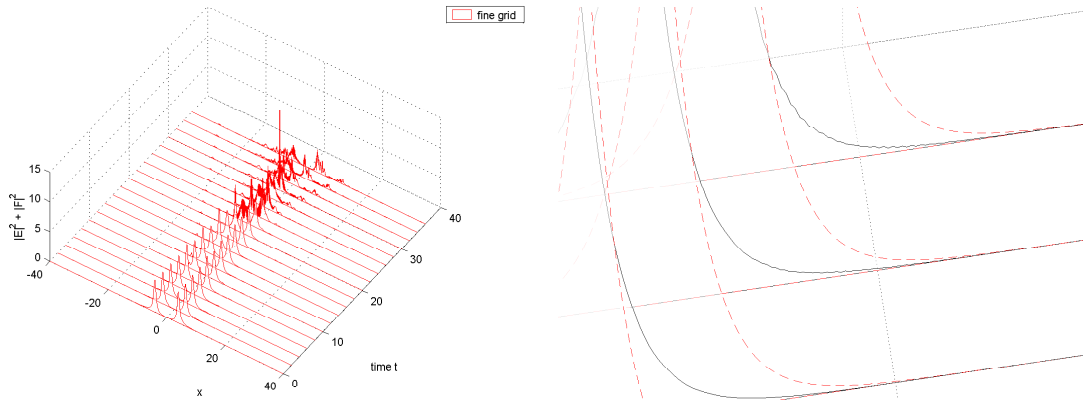

(a) (b)

Figure 4: In a) one can see that for many time steps the method is unstable. At the time $t = 22$ there appear high frequency oscillations with a wavelength of the order of h. The sharp spikes in the energy evolution of the centered FD formula splitting method (Figure 5 a)) are an artifact of that instability. In b) one can see beginning oscillations in a zoomed snapshot of Figure 5 e).

5.3 The Error Convergence in h

Since we have used a 2^{nd} order stencil for the spatial discretization we expect that the error converges at least quadratically. It turns out that the convergence is approximately of 4^{th} order in the L^2-norm and 6^{th} order in the H^1-norm (Figure 6).

The L^2 error is computed as

$$\frac{1}{N}\sum_k |\tilde{E}_k - E_k|^2 + |\tilde{F}_k - F_k|^2 \,, \tag{33}$$

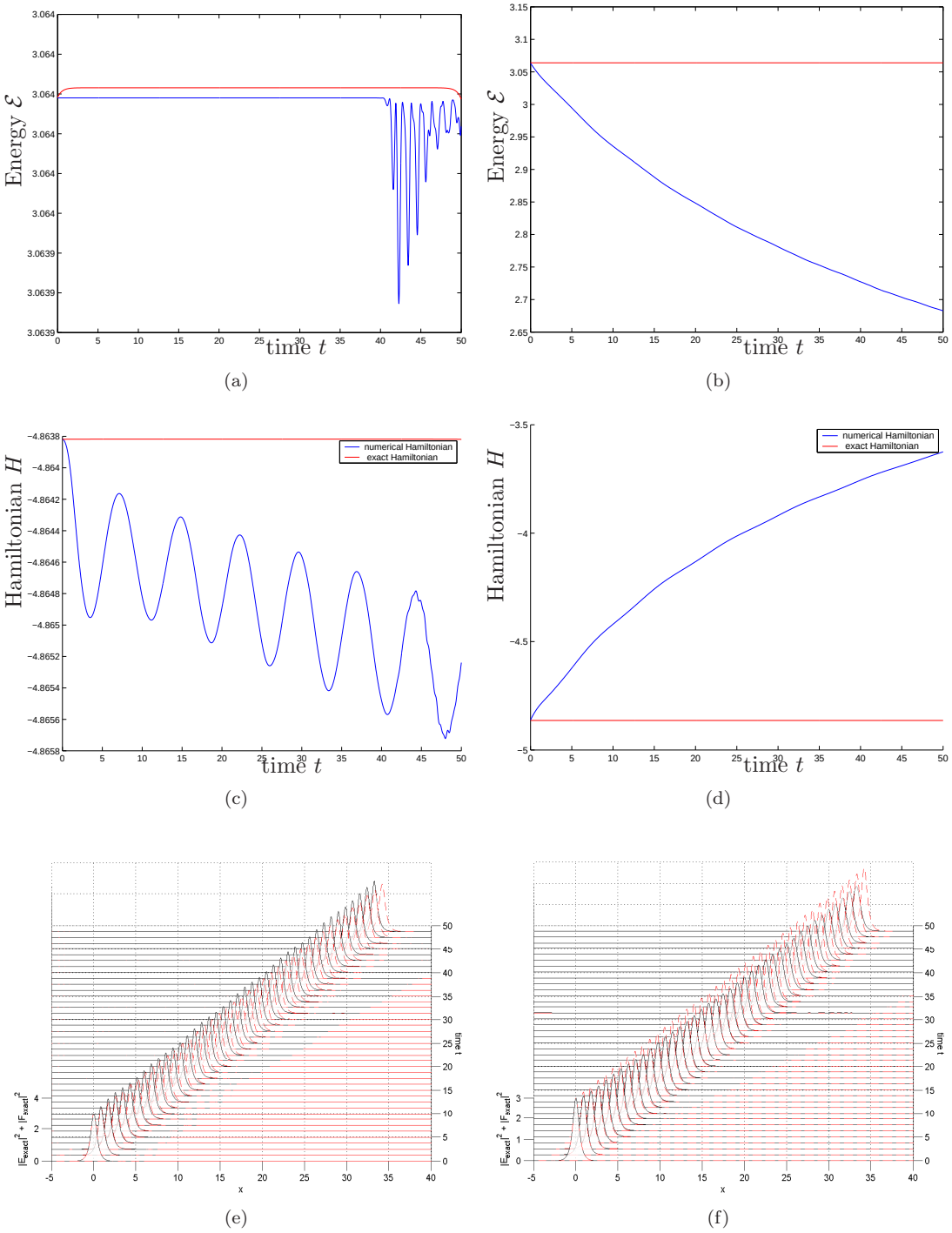

Figure 5: One can see the evolution of energy $\mathcal{E}$ and Hamiltonian H for a single propagating gap solition. On the left side are the results from the centered FD splitting method and on the right side those of the upwinding FD splitting method. In both cases the parameters are set as $v = 0.7$, $\delta = 0.6\pi$ $t = 50$, number iterations =2000, $N = 1000$, x_left=-5, x_right=40. The dashed lines represent the exact solution.

and the H^1 error as

$$\frac{1}{N}\sum_k |\tilde{E}_k - E_k|^2 + |A_k((\tilde{E}_{k+1} - E_{k+1}) - (\tilde{E}_k - E_k)) + B_k((\tilde{E}_k - E_k) - (\tilde{E}_{k-1} - E_{k-1}))|^2$$
$$+|\tilde{F}_k - F_k|^2 + |A_k((\tilde{F}_{k+1} - F_{k+1}) - (\tilde{F}_k - F_k)) + B_k((\tilde{F}_k - F_k) - (\tilde{F}_{k-1} - F_{k-1}))|^2 \,, \qquad (34)$$

where $\tilde{F}$ resp. $\tilde{E}$ are the exact solutions.

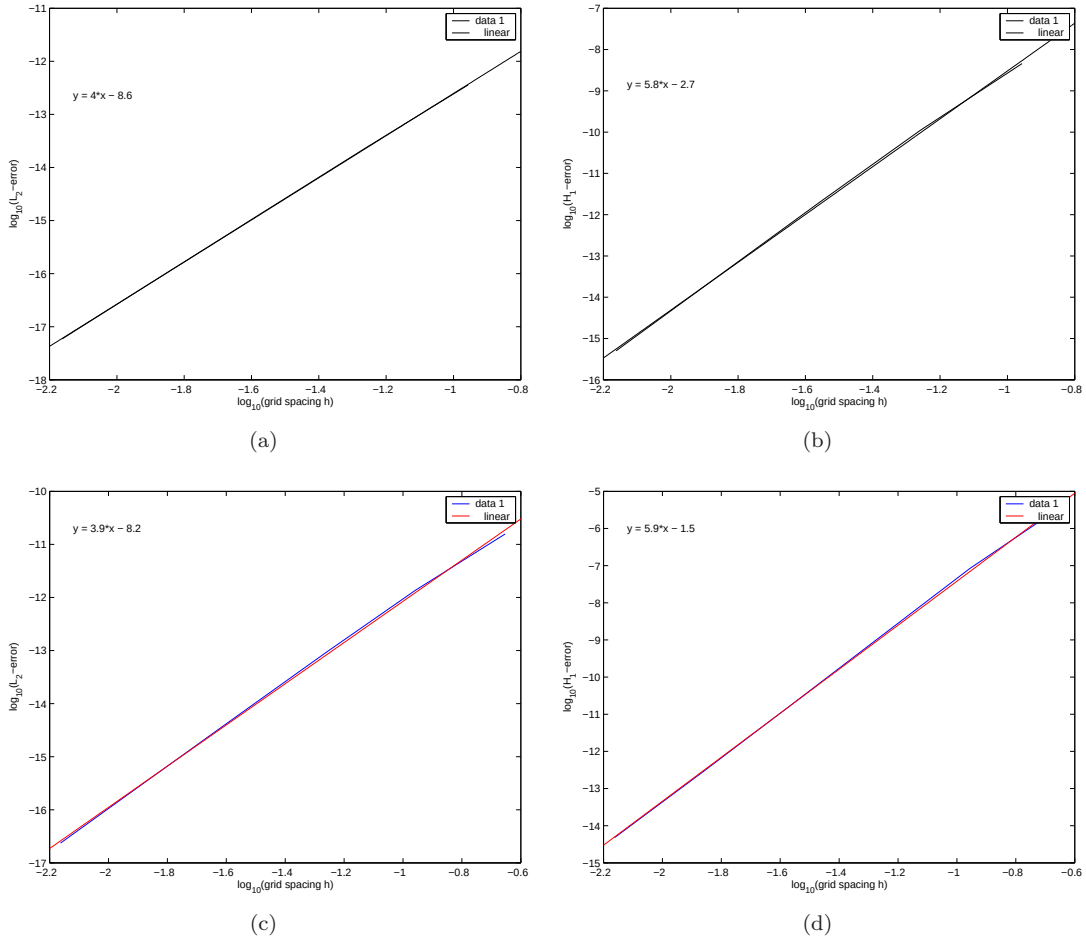

Figure 6: In a) and b) resp. c) and d) the error convergence for the centered FD resp. upwinding FD splitting method is depicted. One can see the error $|E - E_{exact}|^2 + |F - F_{exact}|^2$ in the L^2-norm a)/c) and in the H^1-norm [b)/d)]. The fitting shows that the convergence is approximately of polynomial order 4 in the L^2-norm and 6 in the H^1-norm. Simulation time is 0.00001 in one iteration on the grid $[-10 : h : 12]$. Number of grid points is between 200 and $200 * 2^4$.

5.4 The Error Convergence in dt

For the error convergence in dt we expect also a 2^{nd} order error convergence. The used split step method is of second order if the seperated ODEs can be analytically solved. To solve the linear ODE we use a 2^{nd} order method, i.e. the resulting method should also be of 2^{nd} order. Convergence of the error turns out to be of approximately 4^{th} order (Figure 7).

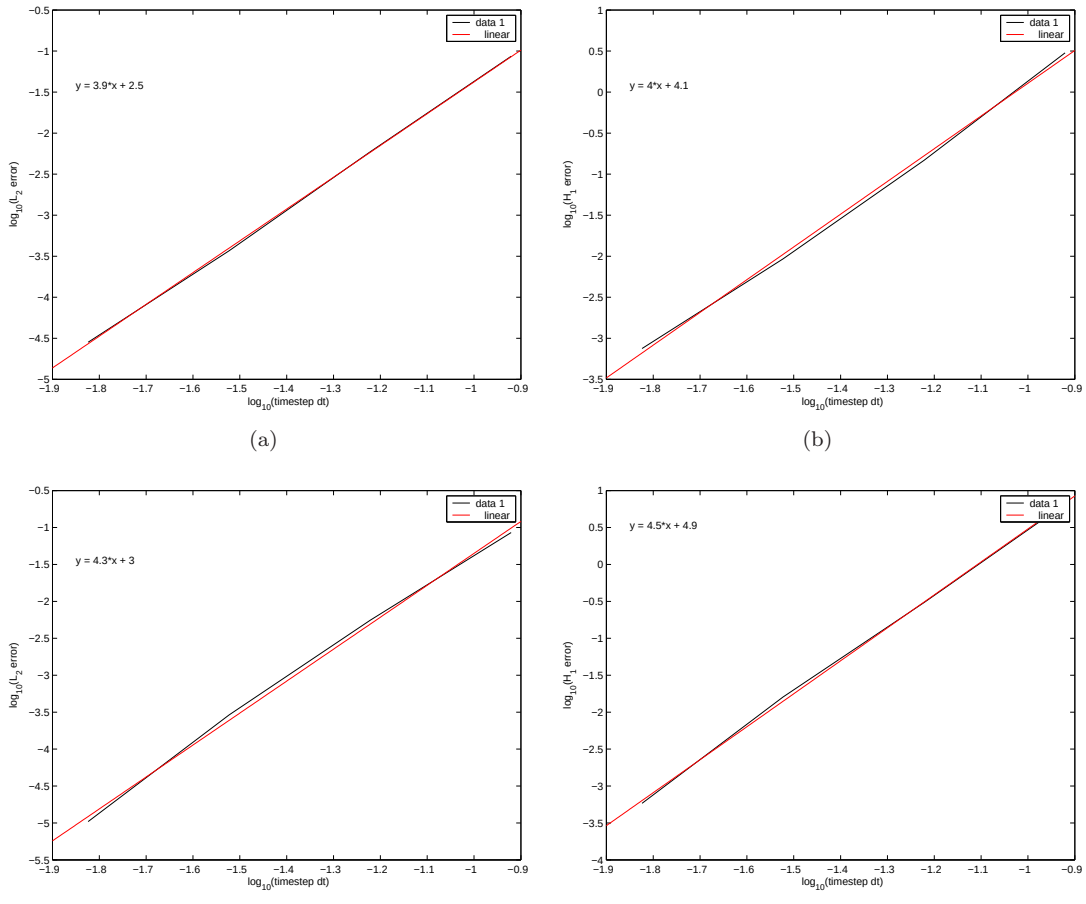

Figure 7: In a) and b) the error convergence in dt for the centered FD formula splitting method is depicted. Instead of the expected 2^{nd} order convergence for both methods we observe approximately 4^{th} order convergence. The used parameters were runtime $t = 6$, number of timesteps $= 50^{[0:4]}$ on a grid with $N = 4000$, x_left=-5, x_right=12;

5.5 Reflection Properties of the Upwinding FD and Centered FD Splitting Method

We test the reflection properties of a single propagating gap soliton. The gap soliton keeps its rough shape but many high frequency oscillation emerge if the method is the centered FD splitting method. In contrast, the upwinding FD splitting method does not produce high frequency oscillation but the rough shape of the soliton is not conserved after the reflection. The upwinding FD splitting method does not produce high amplitude perturbations by reflected radiation. Figure 8 shows a plots for both methods.

5.6 Influence of the Coarseness in Outer Regions on the Solution in the Inner Region

5.6.1 Collision between Two Different Gap Solitons

To produce a lot of radiation by colliding two gap solitons we choose the following parameters: For the left moving gap soliton $v_1 = -0.1$, $\delta_1 = 0.9\pi$ and for the right moving solition $v_2 = 0.01$, $\delta_2 = 0.95\pi$. Simulation time is $t = 56$ in 3640 timesteps. The peaks of both gap solitons have both an offset of 4 from zero. The fine grid reaches from -20 to 20 and has 1024 grid points. The left coarse region goes from -40 to -20 and the right coarse region from 20 to 40. They both have varying number of grid points. We use the notation N_{coarse} for the reduced number of grid points in the "coarse" region and N_{fine} as the number of grid points in the coarse region such that the grid spacing equals the one in the "fine" region.

The analysis of the reflection with the upwinding FD method (Figure 9 and 10) shows that only for very coarse grids in the outer regions strong perturbations on the fine grid can be observed. On the left side of the two Figures the solution with the coarse outer regions while on the right side the error in the inner region are depicted.

Then we computed a reference solution on a uniform fine grid and computed the relative error $\frac{|\tilde{E}-E|^2+|\tilde{F}-F|^2}{|\tilde{E}|^2+|\tilde{F}|^2}$ in the "fine" region in the L^2-norm. This can be seen in Figure 11. For the upwinding FD method, the relative error is negligible for even rather coarse grids. However, how much radiation is reflected into the fine grid region also depends on the method (5.5) and it is possible that other methods produce more backscattered radiation than the upwinding FD splitting method.

5.7 Discrepancy between the upwinding FD method and the method used in Ref. [1]

There is a qualitative difference between the behavior computed with our upwinding FD splitting method and the pseudospectral method on a uniform grid used in Ref. [1]. Colliding gap solitons with parameters $\delta = 0.2\pi$ and $v_G = 0.1$ did not result in the merger of the gap solitons. The reason for that is likely the dissipative nature of the upwinding FD method.

6 Summary

We have tested several numerical methods to solve the NLCME. The two splitting method variants are 4^{th} order in dt and h in the L^2-norm that give similarly good or better results compared to Runge-Kutta methods in terms of conservation of energy $\mathcal{E}$ and Hamiltonian H. Since the centered FD splitting method turns out to be instable we use the upwinding FD splitting method for long runtimes. For the upwinding FD splitting method rather coarse outer regions gave good results compared to a uniformly fine grid, i.e. to obtain a relative error of 1% the grid in the outer region must only have a grid density that deviates from the fine grid by a factor of approximately 2^7. However, the method is not ideally suited for our purposes since reflected radiation does not keep its original pulse shape and the bad conservation properties of the Hamiltonian H and the energy $\mathcal{E}$ compared to the centered FD splitting method. Additionallly, it gives qualitatively different results compared to Ref. [1] which is probably an effect of the dissipative nature of the upwinding FD method.

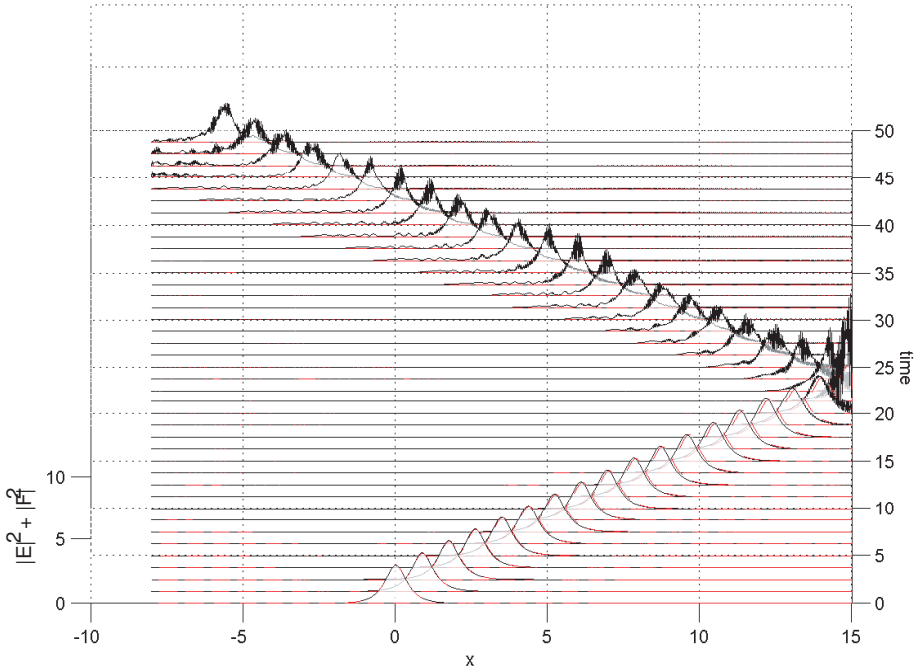

(a)

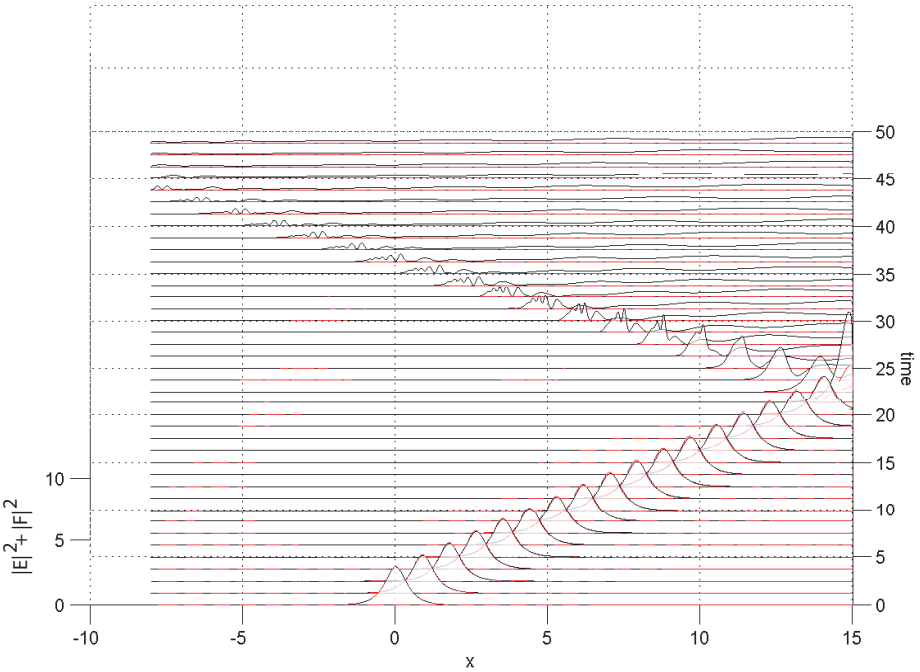

(b)

Figure 8: In a) one can see the reflection behavior of a singe gap soliton computed with the centered FD splitting method. In b) the reflection computed with the upwinding FD splitting method is depicted. The dashed (red) line is the exact solution and the black (solid) line is the numerical solution.

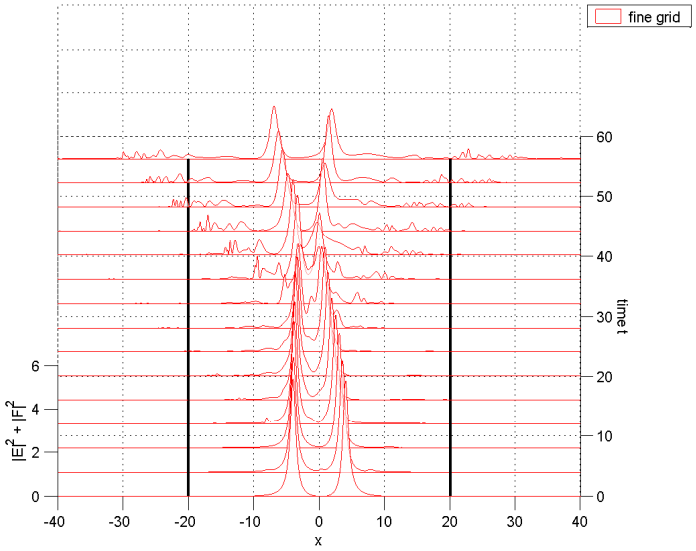

(a)

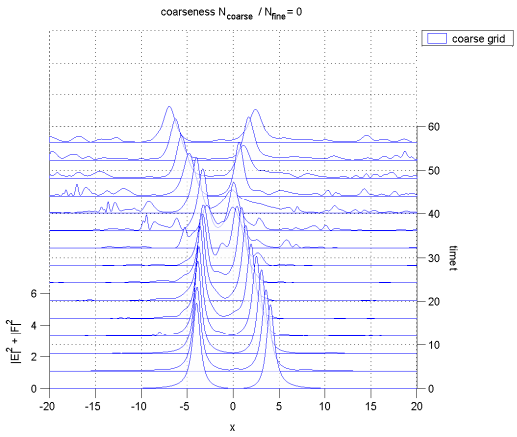

(b)

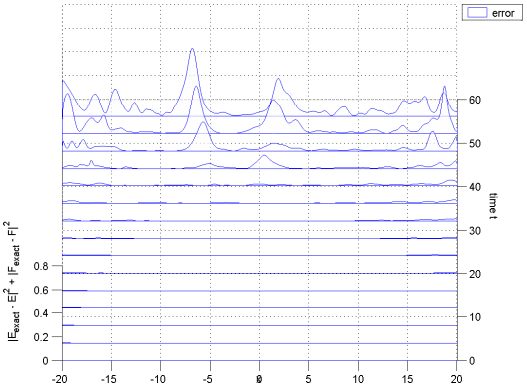

(c)

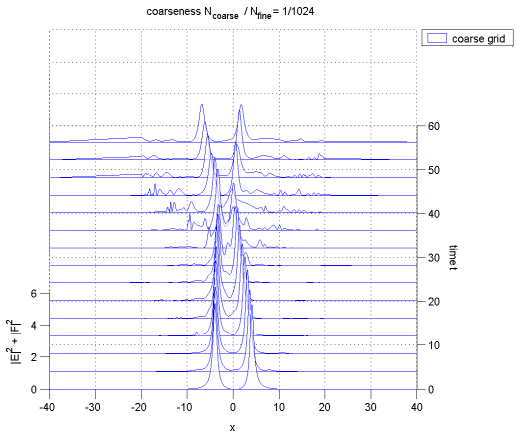

(d)

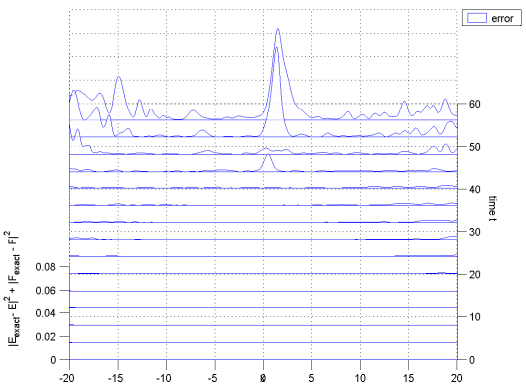

(e)

Figure 9: In a) one can see the reference solution computed on a uniform grid. For all plots the region from $[-20 : 20]$ holds a fine grid with 1024 grid points. The outer coarse regions have $1024\frac{N_{\text{coarse}}}{N_{\text{fine}}}$ grid points, where $\frac{N_{\text{coarse}}}{N_{\text{fine}}} \in \{2^{-[0:10]}, 0\}$. On the left side the solution is depicted and on the right the corresponding error distribution can be seen.

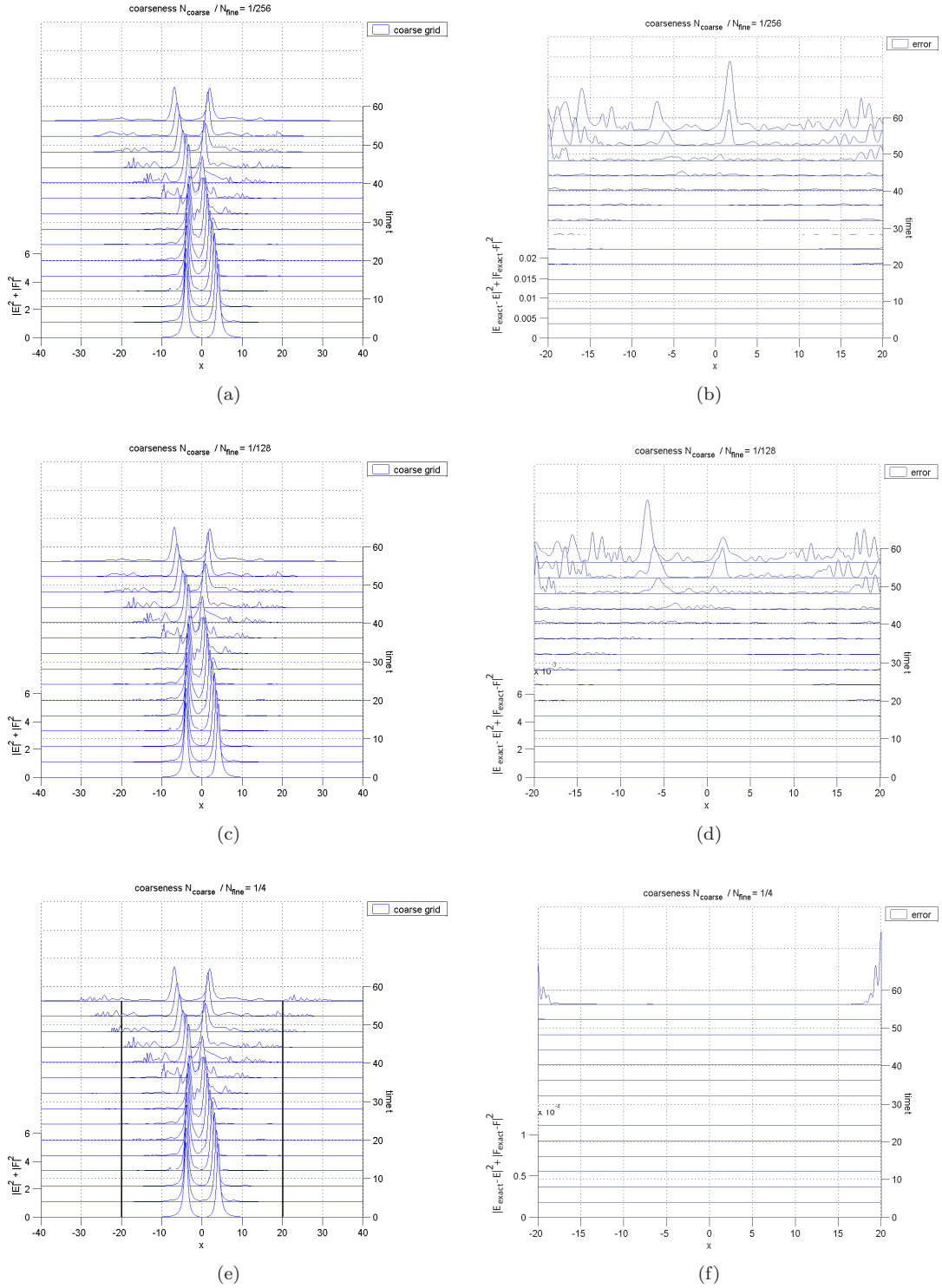

(a) (b)

(c) (d)

(e) (f)

Figure 10: On the left side the solution is depicted and on the right the corresponding error distribution can be seen.

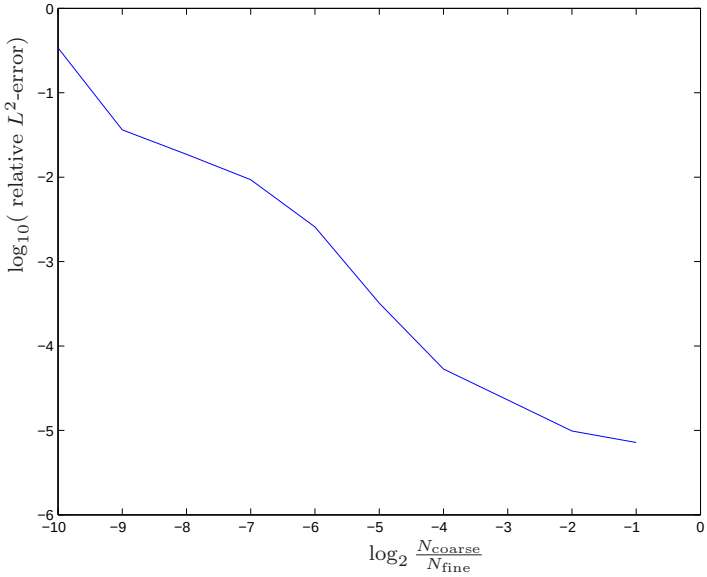

Figure 11: The relative error between the solution computed on the fine grid covering $[-40 : 40]$ and the solution where in the region $[-40 : -20]$ and $[20 : 40]$ a coarser grid with only the fraction N_coarse/N_fine as many grid points in the outer regions is used.

References

[1] William C. K. Mak, Boris A. Malomed, Pak L. Chu **Formation of a Standing-Light Pulse through Collision of Gap Solitions**, arxiv:nlin.PS/0304023 v1

[2] Roy H. Goodman, Michael I. Weinstein, Philip J. Holmes **Nonlinear Propagation of Light in One Dimensional Periodic Structures**, arXiv:nlin.PS/0012020 v3

[3] N.M. Litchinister, B.J. Eggleton, C.M. de Sterke, A.B. Aceves, Govind P. Agrawal **Interaction of Bragg solitions in fiber gratings**, J. Opt. Soc. Am. B/Vol. 16, No. 1 , January 1999

[4] J. W. Thomas **Numerical Partial Differential Equations, Finite Difference Methods**, Springer

[5] E. Hairer, C. Lubich, G. Wanner **Geometric Numerical Integration, Structure-Preserving Algorithms for Ordinary Differential Equations**, Chapter II.5 Splitting Methods , Chapter VI.3 First Examples of Symplectic Integrators, Springer

[6] **Nyquist-Shannon Sampling Theorem**, http://en.wikipedia.org/wiki/Shannon-Nyquist_sampling_theorem